Mon. Not. R. Astron. Soc. **337,** 1407–1416 (2002)

Deep spectroscopy of $z \sim 1$ 6C radio galaxies – II. Breaking the redshift–radio power degeneracy

K. J. Inskip,[1⋆] P. N. Best,[2] H. J. A. Röttgering,[3] S. Rawlings,[4] G. Cotter[1] and M. S. Longair[1]

[1]*Cavendish Laboratory, Madingley Road, Cambridge CB3 0HE*
[2]*Institute for Astronomy, Royal Observatory Edinburgh, Blackford Hill, Edinburgh EH9 3HJ*
[3]*Sterrewacht Leiden, Postbus 9513, 2300 RA Leiden, the Netherlands*
[4]*Department of Astrophysics, University of Oxford, Keble Road, Oxford OX1 3RH*

Accepted 2002 August 22. Received 2002 August 22; in original form 2002 May 8

ABSTRACT

The results of a spectroscopic analysis of 3CR and 6C radio galaxies at redshift $z \sim 1$ are contrasted with the properties of lower-redshift radio galaxies, chosen to be matched in radio luminosity to the 6C sources studied at $z \sim 1$, thus enabling the redshift–radio power degeneracy to be broken. Partial rank correlations and principal component analysis have been used to determine which of redshift and radio power are the critical parameters underlying the observed variation of the ionization state and kinematics of the emission-line gas.

[O II]/Hβ is shown to be a useful ionization mechanism diagnostic. Statistical analysis of the data shows that the ionization state of the emission-line gas is strongly correlated with radio power, once the effects of other parameters are removed. No dependence of ionization state on cosmic epoch is observed, implying that the ionization state of the emission-line gas is solely a function of the properties of the active galactic nucleus rather than the host galaxy and/or environment.

Statistical analysis of the kinematic properties of the emission-line gas shows that these are strongly correlated independently with both redshift and radio power. The correlation with redshift is the stronger of the two, suggesting that host-galaxy composition or environment may play a role in producing the less extreme gas kinematics observed in the emission-line regions of low-redshift galaxies.

For both the ionization and kinematic properties of the galaxies, the independent correlations observed with radio size are stronger than with either radio power or redshift. Radio source age is clearly a determining factor for the kinematics and ionization state of the extended emission-line regions.

Key words: galaxies: active – galaxies: evolution – galaxies: ISM – radio continuum: galaxies.

1 INTRODUCTION

Powerful radio sources are typically associated with massive ellipticals, and are often observed to have extended emission-line regions aligned along the radio source axis. The luminosity and kinematic properties of the emission-line regions are generally observed to be more extreme for radio sources at high rather than at low redshifts. It is important to establish exactly how the properties of the extended emission-line regions (ionization mechanism, kinematics and physical extent) are functions of redshift, radio power and radio size. This will add to our understanding of these complex systems.

⋆E-mail: kji@mrao.cam.ac.uk

Baum & McCarthy (2000) carried out a spectroscopic study of a sample of 52 radio galaxies covering a large range of redshifts, most of which are selected from the 3CR sample. Their analysis of the kinematic and morphological properties of these objects demonstrated a number of important correlations. The kinematic properties of the emission-line gas in these sources were found to vary strongly with redshift and/or radio power, the higher-redshift galaxies generally displaying greater linewidths and velocity amplitudes. The inferred mass of ionized gas and the enclosed dynamical gas were also seen to increase with redshift. Although jet–cloud interactions are not excluded by the data, Baum & McCarthy preferred a gravitational origin for the observed kinematics.

Best, Röttgering & Longair (2000a,b) carried out a study of the emission-line regions of high-redshift 3CR galaxies at $z \sim 1$. Small

radio sources (those with a radio size $D_{\rm rad} < 120$ kpc) were observed to exist in a lower ionization state, and to possess more distorted velocity profiles and boosted low-ionization (e.g. [O II]) emission-line luminosities in comparison with larger radio galaxies ($D_{\rm rad} > 120$ kpc). Their spectra were consistent with small radio sources being predominantly shock-ionized, and large radio sources photoionized by the active galactic nucleus (AGN). Emission-line regions were generally larger in spatial extent in the smaller radio sources. The kinematic and ionization properties of these emission-line regions were also found to be strongly correlated.

Best et al. (2000a,b) also compared the properties of the emission-line regions of high-redshift 3CR galaxies at $z \sim 1$ with a sample of low-redshift 3CR galaxies with $z \lesssim 0.2$ (from Baum, Heckman & van Breugel 1992). Similar radio size trends were observed in the low-redshift sample, although some trends with either radio luminosity and/or redshift were also observed. Line luminosities and equivalent widths were generally less extreme in the low-redshift sources. Tadhunter et al. (1998) showed that a similar correlation exists between line luminosity and radio luminosity in a subsample of 2-Jy sources from the sample of Wall & Peacock (1985). Assuming a simple quasar illumination model, the observed ionization state of the emission-line gas implied that this correlation could not be explained by a simple increase in the flux of ionizing photons associated with more powerful AGN at higher redshifts. The observations could however be reconciled with the simple photoionization model if emission-line region cloud density is enhanced at higher redshifts, as a result of either changes in the host-galaxy environment or radio source shocks increasing in importance.

The flux-limited 3CR sample suffers, however, from Malmquist bias: the strong correlation between redshift and radio power in a flux-limited sample prevents the effects of changes in these two parameters from being disentangled from each other. This degeneracy needs to be broken, in order to determine to what extent changes in redshift and/or the host-galaxy environment, in particular any possible variations in the size and structure of the emission-line regions and the density of the intergalactic medium (IGM), influence the ionization and kinematics of the extended emission-line regions of these galaxies. Higher radio power galaxies generally have intrinsically more powerful jets; the bulk kinetic power of the radio jets has been shown to be strongly correlated with narrow-line region luminosities (Rawlings & Saunders 1991). It is important that we fully understand the effects of changes in radio power on the ionization state and kinematic properties of the extended emission-line regions (EELRs).

Over recent years we have been involved in an ongoing programme of multiwavelength observations investigating a subsample of 11 6C radio galaxies (Eales 1985; Best et al. 1999; Inskip et al. 2002, hereafter Paper I). These sources were selected in order to be well matched to a previously well-studied subsample of 28 3CR galaxies with redshift $z \sim 1$ (Longair, Best & Röttgering 1995; Best, Longair & Röttgering 1996, 1997; Best, Röttgering & Longair 1998; Best et al. 2000a,b). In Paper I the results of deep spectroscopic observations of eight of these sources using the William Herschel Telescope (WHT) were presented. We refer the reader to Paper I for details of sample selection, observations and data reduction, reduced one- and two-dimensional spectra, tabulated line fluxes and composite spectra. Also included in Paper I is a discussion of the kinematic and ionization properties of the 6C galaxies, contrasting them with those of the spectroscopic sample of 3CR galaxies at $z \sim 1$.

The major results of Paper I are briefly summarized below:

(i) The kinematical properties of the EELRs of 6C galaxies are similar to those of the more powerful 3CR sources studied at the same redshift. Small radio sources generally possess more extensive emission-line regions with a more distorted velocity profile and more extreme kinematics than those of larger radio sources.

(ii) [O II] emission-line luminosity is anticorrelated with the size (or age) of the radio source.

(iii) Ionization state varies similarly with radio size for both subsamples, despite the decrease in radio power of the 6C sources. This is interpreted as being due to a changing contribution of ionizing photons from the shock front associated with the expanding radio source. The optical/ultraviolet spectra of the EELRs associated with large radio sources are dominated by photoionization by the AGN and those of small sources by shocks.

There is a great deal of evidence that shocks associated with the expanding radio source play a major role in creating the extreme gas kinematics observed in the spectra of radio galaxies. In addition to the results outlined above, the extreme linewidths observed in the extended emission-line regions are coincident with the radio source structures. This argues against the gravitational origin for the observed kinematics of the gas preferred by Baum & McCarthy (2000), at least for the more extreme sources.

In this paper we compare the results of the 3CR and 6C $z \sim 1$ subsamples with lower-redshift 3CR sources, selected to have similar radio powers to those in the 6C subsample. By considering samples of galaxies covering a larger region of the P–z plane (where P is the radio luminosity of the galaxies), we are able to break the degeneracy between redshift and radio power.

The structure of the paper is as follows. In Section 2, we discuss the selection of low-redshift galaxies for comparison with the $z \sim 1$ 3CR and 6C subsamples. The results of our comparison between low- and high-redshift sources are presented in Section 3, and discussed in Section 4. Conclusions are drawn in Section 5.

Values for the cosmological parameters $\Omega_0 = 0.3$, $\Omega_\Lambda = 0.7$ and $H_0 = 65$ km s^{-1} Mpc^{-1} are assumed.

2 SELECTION OF THE LOW-REDSHIFT SAMPLE

The comparison of the 6C spectroscopic data with those of a more powerful sample of 3CR galaxies at the same redshift gives us an insight into the variation of the ionization states and kinematical properties of radio galaxies with radio power. By selecting another subsample of galaxies at lower redshift, matched in radio power to the 6C subsample at $z \sim 1$, we can investigate the dependence of these galaxy properties with redshift alone, as the combination of three such samples breaks the P–z degeneracy. Unfortunately there are no data available in the literature exactly matching our criteria of full ionization and kinematic data for a large number of galaxies matched in radio power to the 6C subsample. The low-redshift data used in this paper have therefore been taken from two different samples: ionization data from the sample of Tadhunter et al. (1998), and the low-redshift kinematic data from the sample of Baum & McCarthy (2000).

For ionization studies we have selected narrow-line radio galaxies from the steep-spectrum selected subsample of Tadhunter et al. (1993), which is itself taken from the 2-Jy sample of Wall & Peacock (1985). The Tadhunter sample includes all sources from the Wall & Peacock sample with 2.7 GHz flux density >2 Jy, declinations

$\delta < 10°$ and redshifts $z < 0.7$. Whilst the full 2-Jy sample is not spectroscopically complete, the remaining objects without identified redshifts are very faint, and unlikely to lie within the $z < 0.7$ subsample of Tadhunter et al. (1993). This upper redshift limit is also the lower redshift limit of the spectroscopic subsample of 3CR galaxies of Best et al. (2000a), which spanned the redshift range $0.7 < z < 1.25$. The 18 sources selected have both [O III]/[O II] and [O III]/Hβ line ratios available, as presented by Tadhunter et al. (1998). Eight of these sources lie in a similar radio luminosity range to the 6C $z \sim 1$ subsample, and thus can be used in a statistical comparison with the high-redshift sources. Two sources were excluded on the basis of incomplete emission-line information, but neither of these would have fallen in the luminosity range selected for comparison to the 6C galaxies. The sources included in the statistical comparison subsample are 0023−26, 0039−44, 0859−25, 1306−09, 1934−63, 2250−41, 2314+03 (3C 459) and 2356−61. The full subsample of 18 galaxies is 90 per cent complete, and unbiased. Although this sample provides ionization data suitable for comparison with the $z \sim 1$ subsamples, we need to look elsewhere for the kinematics of low-redshift radio sources.

Baum & McCarthy (2000) provide an analysis of the kinematical and morphological properties of a sample of 52 radio galaxies. Their sample is a compilation of two other samples: low-redshift galaxies are taken from the samples of Baum, Heckman & van Breugel (1990) and Baum et al. (1992) and the intermediate- to high-redshift galaxies from the sample of McCarthy, Baum & Spinrad (1996). Both of these were drawn in turn from the emission-line imaging survey of Baum et al. (1988) and imaging by McCarthy, Spinrad & van Breugel (1995). The Baum & McCarthy sample is slightly biased against sources with small emission-line regions, particularly at higher redshifts; at redshifts greater than ∼0.2, it includes most 3CR sources with emission-line imaging sizes greater than 5 arcsec. For comparison with the kinematical properties of $z \sim 1$ radio galaxies, we have selected 22 Fanaroff–Riley type II (FRII) galaxies from the sample of Baum & McCarthy (2000). These are all FRII sources with redshifts of $z < 0.7$, the same upper redshift limit as used in the Tadhunter et al. subsample. Of the 22 galaxies selected, 21 have a measured full width at half-maximum (FWHM), but only eight are used in statistical comparisons with the 6C galaxies at $z \sim 1$, as these have similar radio luminosities. These are the sources 3C 79, 3C 169.1, 3C 299, 3C 300, 3C 306.1, 3C 337, 3C 435 and 3C 458.

Fig. 1 shows the radio power versus redshift distribution of the four samples considered in this paper, illustrating which of the low-redshift galaxies are suitable for comparison with the $z \sim 1$ 6C and 3CR subsamples.

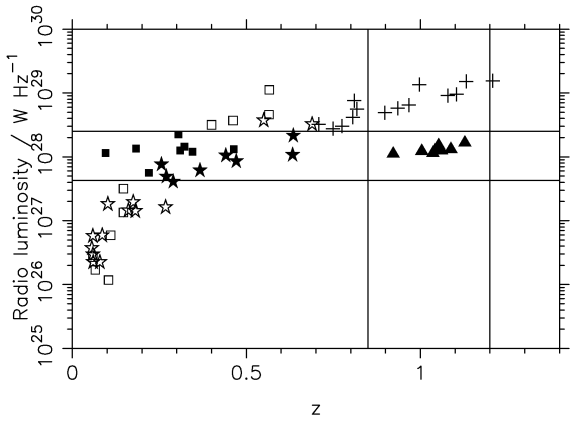

Figure 1. *P–z* diagram illustrating the selection of low-redshift galaxies. The 3CR $z \sim 1$ subsample radio galaxies are represented by crosses, and the 6C radio galaxies by solid triangles. The vertical lines delineate the redshift range from which the 6C subsample was selected, and the horizontal lines the range in radio luminosity within which low-redshift sources will be directly compared with 6C sources. The Baum & McCarthy low-redshift subsample radio galaxies are represented by filled and open stars, and the Tadhunter et al. sample radio galaxies by filled and open squares, the filled symbols representing the luminosity-matched low-redshift data used in the statistical comparisons.

3 COMPARISON WITH GALAXIES AT LOW REDSHIFT

3.1 The ionization state of the emission-line gas

3.1.1 [O II]/Hβ as a diagnostic test

For the Tadhunter et al. (1998) subsample, the line ratios [O III]/[O II] and [O III]/Hβ are available. These can be used to determine [O II]/Hβ, a line ratio that can be inferred for the $z \sim 1$ data based on our measurements of [O II] and Hγ or other Balmer lines, assuming the Balmer line ratios for case B recombination. The composite spectra produced for the $z \sim 1$ samples (Paper I) suggest that this line ratio is quite different for large and small radio sources, and thus may be a useful diagnostic of the ionization mechanism. To investigate this, we used the MAPPINGSII (Sutherland et al. 1993) results for [O II]/Hβ and C III] 1909 Å/C II] 2326 Å to create a new ionization mechanism diagnostic diagram (Fig. 2).

Marked on the diagram are the predictions of shock (Dopita & Sutherland 1996) and photoionization models (Binette, Wilson & Storchi-Bergmann 1996; Allen, Dopita & Tsvetanov 1998 ; digitized data kindly provided by Mark Allen). The 6C and 3CR data points are also included. Where Hγ, Hδ or Hζ could not be measured in our spectra, an upper limit was determined for the Hβ flux for these sources. In these cases, the [O II]/Hβ line ratio is given as a lower limit. No correction has been made for internal extinction. Assuming similar levels of internal extinction to that measured for Cygnus A (Osterbrock 1989), this is likely to have only a minimal impact on our results.

The diagnostic plot in Paper I utilized the predictions of the line ratios C III] 1909 Å/C II] 2326 Å and [Ne III] 3869 Å/[Ne V] 3426 Å for these models. Large sources were generally well matched to pure photoionization by the AGN, with an ionization parameter $-2 \lesssim \log_{10} U \lesssim -1$ and spectral index $\alpha = -1$. Small sources fitted well the predictions of the shock models incorporating precursor ionization regions. Alternatively, the photoionization models combining matter-bounded and ionization-bounded clouds of Binette et al. (1996) also seemed to provide a good fit to the data, with the smaller radio sources typically having a smaller fraction of matter-bounded clouds. The positions of the data points in relation to the different models can be compared between Fig. 2 and the diagnostic plot from Paper I, allowing the consistency of the models in fitting the observed data to be gauged.

When comparing two or more line ratio diagnostic diagrams, it quickly becomes apparent that not all the models explain the spectra of the observed sources consistently from one plot to another. However, some of the modelled tracks appear to fit the data reasonably well on both plots. The five 'photoionized' sources on the diagnostic plot in Paper I appear close to the predicted line ratios of the same model in Fig. 2. Most of the points that were previously well matched by the predictions of the shock plus precursor region

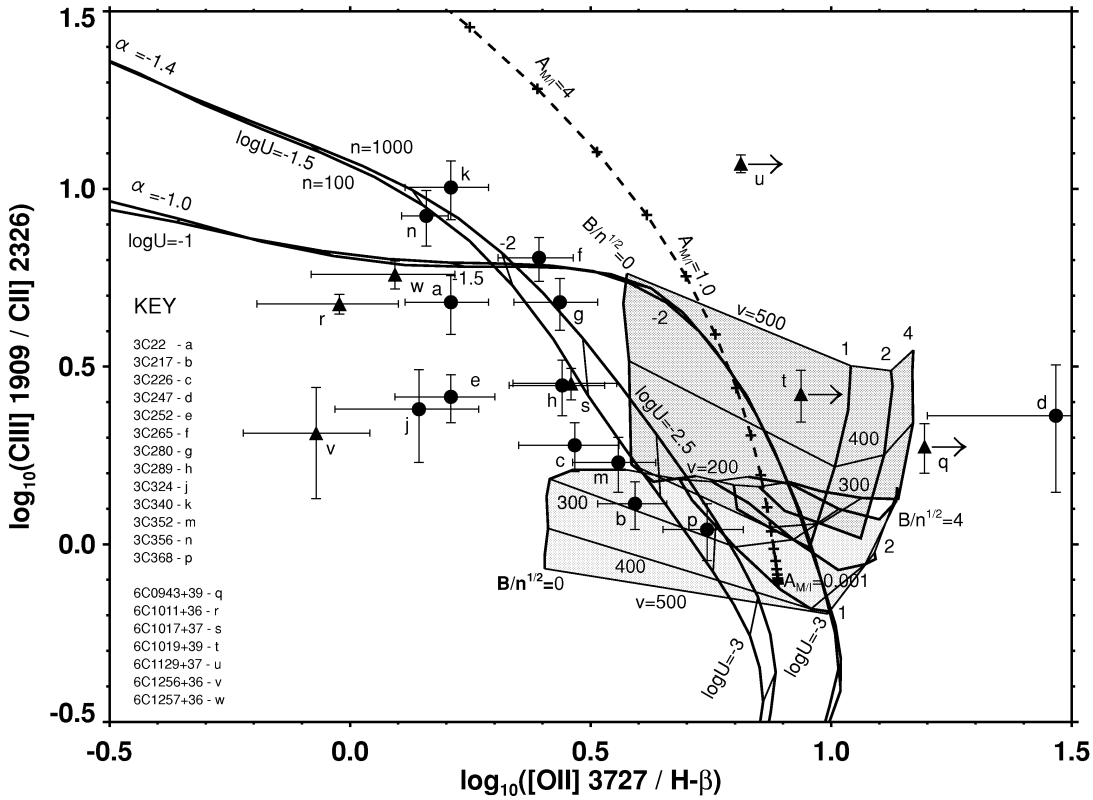

Figure 2. An [O II]/Hβ versus C III] 1909-Å/C II] 2326-Å emission-line ratio diagnostic diagram for 6C and 3CR galaxies at $z \sim 1$. Points are plotted for each galaxy (3CR galaxies are represented by circles and 6C galaxies by triangles), and compared with the theoretical predictions for shock ionization, simple photoionization, and photoionization including matter-bounded clouds. The shock ionization line ratio predictions are those of the models of Dopita & Sutherland (1996). Results both for simple shock ionization (light shading) and for models including a precursor ionization region (dark shading) are included on the diagram. Shock velocities were allowed to vary between 150 and 500 km s^{-1}. The 'magnetic parameter', $B/\sqrt{n}$, which controls the effective ionization parameter of the post-shock gas, was varied from 0 to 4 μG cm$^{-1.5}$. The simple photoionization model tracks are taken from the theoretical line ratios calculated using the MAPPINGSII code (Sutherland et al. 1993; Allen et al. 1998; Mark Allen, private communication). A power-law spectrum illumination ($F_\nu \propto \nu^\alpha$, $\alpha = -1$ or -1.4, with a high-energy cut-off at 1.36 keV) of a planar slab of material ($n_e = 100$ or $1000\,\mathrm{cm}^{-3}$) was assumed, with an ionization parameter $10^{-4} \leqslant U \leqslant 1$. The models correspond to cloud sizes from 0.003 to 32 pc, and are ionization-bounded. Photoionization tracks for the combination of matter-bounded and ionization-bounded clouds are also plotted, using the predicted line ratios of Binette et al. (1996). $A_{M/I}$ represents the ratio of the solid angle from the photoionizing source subtended by matter-bounded clouds relative to that of ionization-bounded clouds. For further details, see Best et al. (2000b).

models remain so in this diagram as well. As a general rule, small sources show lower ionization parameters than larger sources, and their positions on the diagnostic plot are consistent with the predictions of shock ionization. However, the shock ionization and AGN photoionization models cannot be completely separated in Fig. 2. These results clearly illustrate that the power of line ratio plots as a diagnostic of the ionization mechanism is greatly enhanced when several different plots are considered together, as ambiguities on one or more plots may be resolved by additional modelled line ratios.

One clear result from this plot is that the preferred region of the photoionization tracks predicts lower values of [O II]/Hβ than the predictions of the shock models. Thus, the [O II]/Hβ line ratio can provide a suitable indication of any changes of ionization state that may be observed in the low-redshift sources, just as the C III] 1909-Å/C II] 2326-Å line ratio was used to do so in Paper I.

3.1.2 Balmer lines versus [O II] 3727 Å – investigating variation in ionization state in the three samples

In Fig. 3(a) the [O II]/Hβ line ratio data for the Tadhunter et al. (1998) subsample and the two $z \sim 1$ samples are plotted against radio size. Fig. 3(b) displays the variation of this line ratio with radio power for the same samples; Fig. 3(c) plots this parameter against redshift. It is interesting to note that there is a much larger spread in the [O II]/Hβ line ratio for the lower radio power sources.

Spearman rank correlation tests have been carried out for these data and the results tabulated in Table 1. For three 6C sources, the [O II]/Hβ line ratio could only be calculated as a lower limit; these values have been treated as measured values for all statistical analyses unless stated otherwise. However, as the [O II]/Hβ line ratios for these sources are amongst the highest in the samples, the statistics are unlikely to suffer. The line ratios of the galaxies in all three subsamples combined are anticorrelated with radio size at the 99.8 per cent significance level, suggesting that this line ratio is a suitable alternative to C III] 1909 Å/C II] 2326 Å as an indicator of changes in ionization state with radio size. The data are slightly less strongly correlated with radio power and redshift.

We have also carried out partial rank correlations for these galaxies, using the method described by Macklin (1982), which enables the true dependences of the different properties to be determined, by removing the effects of correlations with one or more of any other parameters.

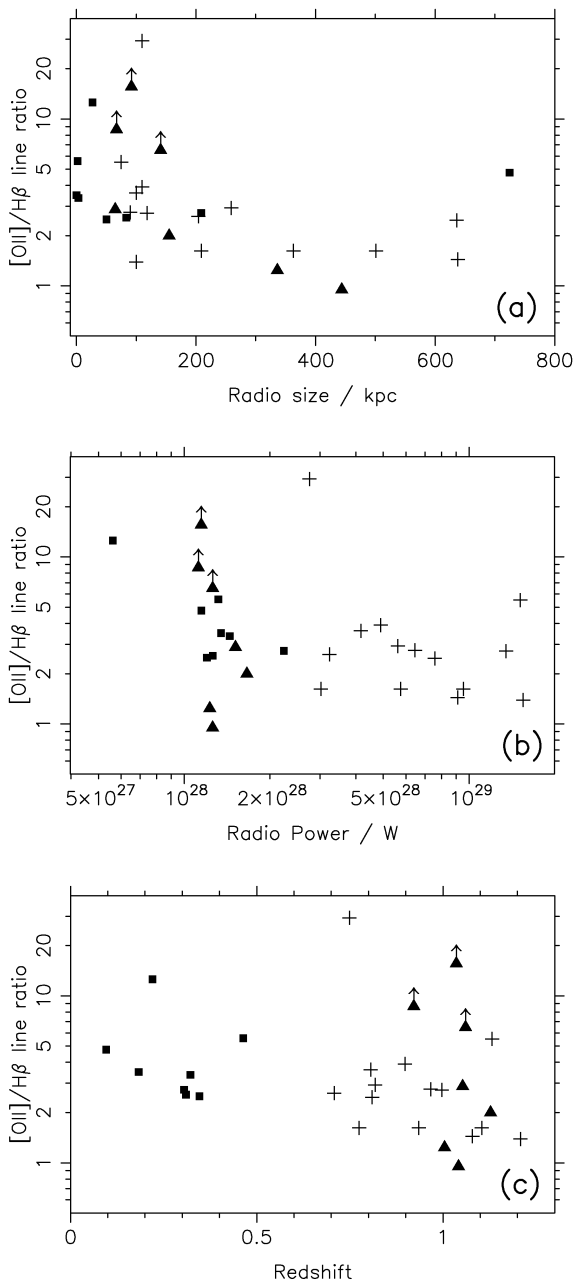

Figure 3. Plot of the [O II]/Hβ line ratio versus (a) radio size, (b) radio power and (c) redshift for three samples. Crosses represent the 3CR $z \sim 1$ subsample galaxies, filled triangles the 6C sources, and the filled squares the Tadhunter et al. sample galaxies matched in radio power to the 6C subsample. The 6C and 3CR data points are plotted as lower limits where the Hβ luminosities are upper limits inferred from Hδ rather than Hγ luminosities.

Our results show strong anticorrelations of the [O II]/Hβ line ratio with both radio size and luminosity (see Table 1). Although a Spearman rank test initially found a significant correlation with redshift, partial rank analysis shows that redshift is an unimportant parameter and the correlation was induced by the strong correlation between z and radio power. We can conclude that there is no strong dependence of ionization state on any changes with redshift in the properties of the host galaxy or its environment.

Another way of determining the most important correlations within a set of data is a principal component analysis (also known as a Karhunen–Loeve transform). This is described by Kendall (1980) and Efstathiou & Fall (1984). For a data set with p variables for each of N parameters, a new set of uncorrelated parameters can be determined (the principal components of the data), which are linear functions of the original variables. If the original variables are standardized to zero mean and unit variance, the principal components will also be independent of each other. The first principal component of the data has the largest possible variance of any linear function, and can be thought of as defining the line of closest fit to the p-dimensional set of N data points, in that the sum of squares of the distances of the data points in any direction from such a line will be minimized. The magnitude of this eigenvector indicates what fraction of the data set can be explained by these correlations alone. The second principal component has the largest variance subject to being uncorrelated (i.e. orthogonal) to the first. Further principal components are uncorrelated with all the preceding principal components.

The results of a principal component analysis of our data are displayed in Table 2, and confirm the results of the partial rank coefficients. This analysis has been carried out twice for the three galaxy subsamples: first using only the low-redshift data matched in radio power to the 6C subsample, and secondly using the full low-redshift subsample. Although there are subtle differences between the two sets of results, the overall correlations determined are the same in both cases.

In both cases, the eigenvector of the first principal component accounts for ∼45 per cent of the variance within the sample, that of the second component ∼30 per cent, the third component ∼20 per cent and the fourth <10 per cent. A positive correlation between P and z is clearly the strongest correlation within the data, being inverted significantly only in the final eigenvector, in order to remove the remaining scatter in the data. The advantage of using the chosen combination of three samples is that the effects of this correlation can be accounted for, and the redshift–radio power degeneracy successfully broken. Anticorrelations of the [O II]/Hβ line ratio with both redshift and radio power are implied by the first principal component. However, the second component reverses and weakens these correlations, particularly for redshift. In the first eigenvector, ionization state and radio size ($D_{\rm rad}$) are seen to be anticorrelated for the matched samples, and very weakly correlated for the full low-redshift sample. The second eigenvector shows a strong anticorrelation between the ionization state and size of the radio source in both cases, suggesting that this is indeed a significant correlation. This difference is perhaps due to an underlying anticorrelation between radio size and either P or z, which weakens the relationship between radio size and the [O II]/Hβ line ratio, although it is unclear from these data whether anticorrelations between either P and $D_{\rm rad}$ or between z and $D_{\rm rad}$ are real. An anticorrelation between $D_{\rm rad}$ and z is observed by Neeser et al. (1995) and Blundell, Rawlings & Willott (1999), and is likely to be due in part to the selection effects inherent within flux-limited samples, which are biased towards smaller sources at high redshift because of Malmquist bias and the decrease in flux density with radio size for individual sources (Kaiser, Dennett-Thorpe & Alexander 1997).

These results are fully consistent with the results of the partial rank correlation tests, and suggest that the following are real: a strong positive correlation between P and z, and weaker anticorrelations between $D_{\rm rad}$ and z or P, due to the selection effects in defining the sample. Anticorrelations between I and P, and between I and $D_{\rm rad}$, are also real, where I represents the [O II]/Hβ line ratio as a measure of the ionization state within the emission-line gas, a large value for I implying a low ionization state. Of the implied

Table 1. Spearman rank correlation coefficients. These are given for the correlations of the emission-line ratio [O II]/Hβ with redshift, radio power and radio size, along with partial rank coefficients for the same parameters. Significance levels for each correlation are also tabulated where these are greater than 80 per cent. I = ionization as indicated by the line ratio [O II]/Hβ, z = redshift, P = radio power and D = radio size. The labelling of the correlations is as follows: r_{Iz} is the correlation coefficient for ionization state versus redshift; $r_{Iz|D}$ is the partial correlation coefficient, removing correlations with radio size from any correlation between ionization state and redshift; and $r_{Iz|PD}$ is the partial correlation coefficient for ionization state and redshift after correlations with both radio size and radio power have been removed. Other correlation coefficients are labelled similarly.

	Ionization correlations		
	with redshift	with radio power	with radio size
3C at $z\sim1$ ($n=14$)	$r_{Iz}=-0.338$ (-88%)	$r_{IP}=-0.369$ (-90%)	$r_{ID}=-0.555$ (-98%)
6C at $z\sim1$ ($n=7$)	$r_{Iz}=-0.214$	$r_{IP}=-0.505$ (-88%)	$r_{ID}=-0.750$ (-97%)
Radio power matched low-z 3C ($n=8$)	$r_{Iz}=-0.310$	$r_{IP}=-0.333$	$r_{ID}=-0.310$
All three subsamples ($n=29$)	$r_{Iz}=-0.332$ (-96%)	$r_{IP}=-0.369$ (-98%)	$r_{ID}=-0.525$ (-99.8%)
	$r_{Iz\|P}=0.053$	$r_{IP\|D}=-0.202$ (-85%)	$r_{ID\|z}=-0.256$ (-91%)
	$r_{Iz\|D}=-0.065$	$r_{IP\|z}=-0.238$ (-89%)	$r_{ID\|P}=-0.220$ (-87%)
	$r_{Iz\|PD}=0.051$	$r_{IP\|Dz}=-0.198$ (-84%)	$r_{ID\|zP}=-0.219$ (-86%)
Including the full low-z subsample ($n=38$)	$r_{Iz}=-0.247$ (-93%)	$r_{IP}=-0.256$ (-94%)	$r_{ID}=-0.388$ (-99.2%)
	$r_{Iz\|P}=0.046$	$r_{IP\|D}=-0.194$ (-87%)	$r_{ID\|z}=-0.196$ (-88%)
	$r_{Iz\|D}=-0.076$	$r_{IP\|z}=-0.139$	$r_{ID\|P}=-0.230$ (-91%)
	$r_{Iz\|PD}=0.072$	$r_{IP\|Dz}=-0.192$ (-87%)	$r_{ID\|zP}=-0.236$ (-92%)

Table 2. Principal component analysis of emission-line region ionization state and other radio source parameters. This analysis has been carried out on the two $z\sim1$ subsamples and either the radio power matched or full low-redshift subsamples. The four principal components are linear functions of the parameters, determined such that the first component defines the closest line of fit to the data points. The eigenvectors defining each principal component are given, as are the percentages of the total variance in the data accounted for by each principal component.

Variable	Eigenvectors for the three matched samples				Eigenvectors including the full low-redshift data			
	1	2	3	4	1	2	3	4
I	0.4012	0.5745	0.6905	0.1794	0.1336	0.7273	0.6572	0.1460
z	−0.5413	0.5283	0.0446	−0.6526	−0.6650	−0.0685	0.3561	−0.6530
P	−0.6238	0.2694	−0.0519	0.7319	−0.6972	−0.0225	0.0074	0.7165
D	−0.3961	−0.5642	0.7201	−0.0790	0.2320	−0.6826	0.6643	0.1975
Percentage	44.30	26.43	18.45	10.82	43.28	29.74	19.30	7.68

correlations with ionization state, the [O II]/Hβ line ratio is most strongly anticorrelated with radio size, followed by radio power.

3.2 The Baum & McCarthy sample: kinematics comparison

The first parameter we consider in our comparison of the kinematics of radio galaxies at high and low redshift is the maximum value of the velocity FWHM, which varies with spatial position. This parameter is very robust, easily determined and provides a straightforward measure of the kinematic effects of any shocks associated with jet–cloud interactions. The emission-line gas FWHM is plotted against radio size, radio power and redshift in Fig. 4.

In general, the lower-redshift sources have smaller FWHM than the two high-redshift samples. The FWHM of both 6C and 3CR galaxies are anticorrelated with radio size, whilst the low-redshift galaxies selected from the Baum & McCarthy (2000) sample are not correlated very significantly with this parameter. Baum & McCarthy claim that there is little evidence for an anticorrelation between radio size and the velocity FWHM of the emission-line gas in their complete sample, such as that seen in both $z\sim1$ subsamples. It is not surprising that this result is obtained, as by considering galaxies over their full range of redshifts, any positive correlation between redshift and FWHM such as that observed for our three samples will act to diminish any anticorrelation between radio size and FWHM. Best et al. (2001) separated the full Baum & McCarthy sample into subsamples of sources with $z<0.6$ and $z>0.6$; the high- and low-redshift subsamples each displayed a strong anticorrelation between velocity FWHM and radio size. In the redshift range we consider, the sample is nearly complete for sources with large emission-line regions, and an anticorrelation between FWHM and redshift is observed. Considering all three samples together, FWHM is clearly anticorrelated with radio size, and correlated with redshift and radio power. The strengths of these correlations are listed in Table 3.

As before, some of these correlations may not indicate an intrinsic connection between FWHM and redshift, radio power or radio size, but instead may be due to secondary correlations between these other parameters. This can be disentangled by carrying out partial rank correlation tests on the data, removing the influence of one or more of the other parameters. The partial rank analysis shows that the strongest relationship between the parameters is an anticorrelation with radio size (>99.9 per cent significant), followed by a positive correlation with redshift (>98 per cent significant) and a slightly weaker correlation with radio power (>94 per cent significant). The relative importance of the trends with redshift and radio power can also be observed in Fig. 4. Fig. 4(b) shows that the kinematic properties of the 6C subsample are clearly more extreme than those of the low-redshift 3CR subsample. These samples are

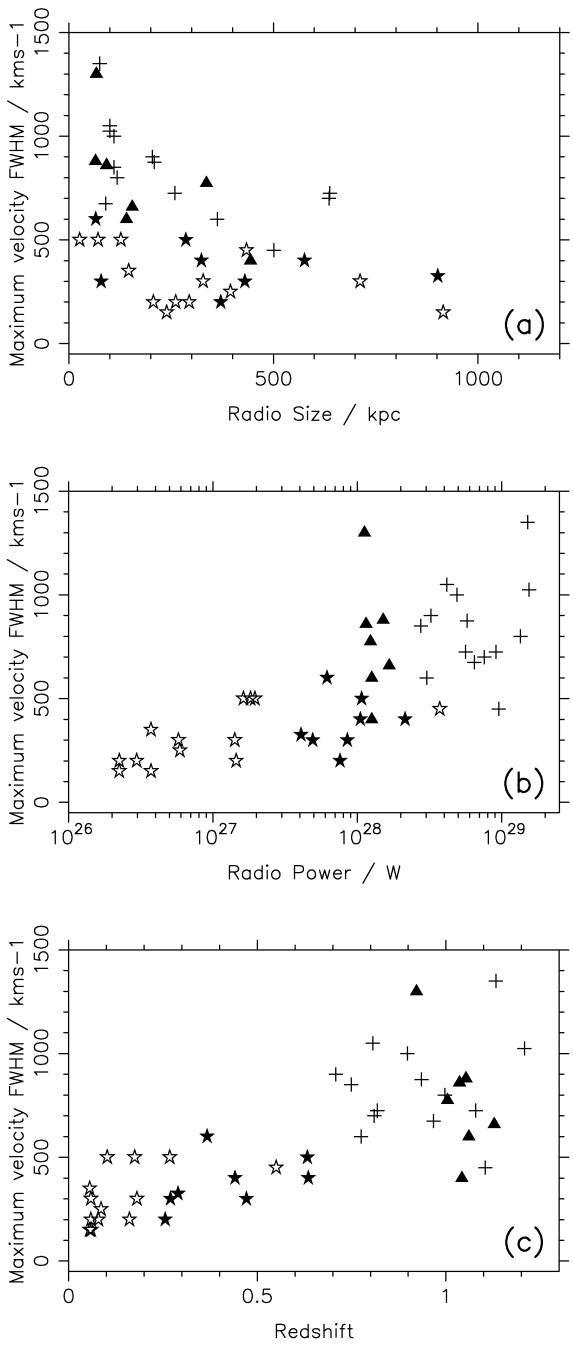

Figure 4. FWHM of galaxies in three samples: (a) FWHM versus radio size; (b) FWHM versus radio power; and (c) FWHM versus redshift. The 3CR $z \sim 1$ subsample galaxies are represented by crosses, and the 6C galaxies by solid triangles. The Baum & McCarthy low-redshift subsample galaxies are represented by filled and open stars, for those galaxies matched in flux to 6C sources and the remainder of the low-redshift sources, respectively.

matched in radio power, but not in redshift. The differences between the ~ 1 6C and 3CR subsamples, matched in redshift but not radio power, are much less obvious, suggesting that the gas kinematics are indeed more strongly dependent on redshift than on radio power.

We have also carried out a principal component analysis for these data sets, the results of which are tabulated in Table 4. The first principal component accounts for over 60 per cent of the variance in the kinematic data. Practically all the scatter in the data can be accounted for with the first two eigenvectors. The reduction in the scatter of the data points compared with the ionization state data provides the first indication that any correlation between P, D or z with the emission region gas FWHM is likely to be much more significant than the correlations observed between these parameters and the ionization state of the gas. The first eigenvector for both data sets gives strong positive correlations between P, z and FWHM, and a strong anticorrelation between each of these parameters and $D_{\rm rad}$. In the second eigenvector the correlation between P and z, and the anticorrelation between FWHM and $D_{\rm rad}$, remain strong, but the other correlations implied by the first eigenvector are reversed and hence greatly weakened (particularly the FWHM–radio power correlation). These results fully confirm those of the partial rank analysis: the most important kinematic correlations are FWHM anticorrelated with radio size, and positively correlated with redshift and radio power, in decreasing order of significance. As for the ionization data, we also observe a correlation of redshift with radio power, as well as an anticorrelation of radio size with redshift.

The variation of velocity range (defined as the difference between the most positive and negative velocity components of the [O II] line) with radio size is plotted in Fig. 5 for all three samples. The distributions of all three samples appear very similar, suggesting that velocity range has no dependence on either redshift or radio power. A visual examination of Fig. 5 suggests that the greatest range of velocities is observed in the smaller radio galaxies. However, a Kolmogorov–Smirnov test, which is more suitable than a Spearman rank test for an analysis of the significance of the suspected trend, shows that the decrease in velocity range with radio size is not significant for any or all of the subsamples combined; nor is the decrease in maximum velocity range from the 3C to 6C sources statistically significant. It can be safely assumed that the velocity range data for any sample is drawn from the same population, regardless of redshift, radio size or radio power.

Another parameter we have studied previously is the luminosity of the [O II] line scaled by the ratio of the radio power of a source to the mean value for the sample, and its variation with radio power (see Paper I). Owing to different observational techniques (long-slit spectroscopy versus narrow-band imaging), a strict comparison between the [O II] luminosities of the low- and high-redshift galaxies is not feasible. None the less there is little variation in scaled $L_{[\rm O\,II]}$ with radio size for the low-redshift sources. A decrease in scaled $L_{[\rm O\,II]}$ with radio size as seen for the $z \sim 1$ data is *not* observed, suggesting that any boosting of line luminosity by shocks in the smaller sources is much less important at lower redshifts. This would be consistent with the less extreme kinematics observed in the low-redshift subsample. If the kinematic results are due in part to radio power/shock strength effects, as found from the strong independent correlation of FWHM with radio power, a weaker or non-existent decrease in $L_{[\rm O\,II]}$ with radio size would also be expected.

4 DISCUSSION

In this paper, we have compared the ionization properties of both the 6C and 3CR subsamples at $z \sim 1$ with the ionization properties of the low- to intermediate-redshift galaxies ($z < 0.7$) in the sample of Tadhunter et al. (1998). We have shown that, whilst not as effective as the C III] 1909-Å/C II] 2326-Å line ratio, [O II]/Hβ can be used as a useful diagnostic of the emission-line ionization mechanism. The [O II]/Hβ ratios of the Tadhunter sample galaxies at low redshift clearly display the same variation between the degree of ionization and the radio source size, or, alternatively, between source age and ionization mechanism. We have contrasted

Table 3. Spearman rank correlation coefficients. These are given for the correlations of the maximum velocity FWHM with redshift, radio power and radio size, along with partial rank coefficients for the same parameters. Significance levels for each correlation are also tabulated where these are greater than 85 per cent. K = FWHM, z = redshift, P = radio power and D = radio size. The labelling of the correlation coefficients is as for Table 1.

Sample	Kinematics correlations with redshift	with radio power	with radio size
3C at $z\sim1$ ($n=14$)	$r_{Kz}=0.079$	$r_{KP}=0.077$	$r_{KD}=-0.650$ (-99.4%)
6C at $z\sim1$ ($n=7$)	$r_{Kz}=-0.536$ (-89%)	$r_{KP}=-0.450$ (-85%)	$r_{KD}=-0.821$ (-99%)
Radio power matched low-z 3C ($n=8$)	$r_{Kz}=0.566$ ($+93\%$)	$r_{KP}=0.325$	$r_{KD}=-0.374$
All three subsamples ($n=29$)	$r_{Kz}=0.520$ ($+99.8\%$)	$r_{KP}=0.570$ ($+99.94\%$)	$r_{KD}=-0.559$ (-99.92%)
	$r_{Kz\|P}=0.410$ ($+99\%$)	$r_{KP\|D}=0.541$ ($+99.88\%$)	$r_{KD\|z}=-0.464$ (-99.4%)
	$r_{Kz\|D}=0.541$ ($+99.88\%$)	$r_{KP\|z}=0.227$ ($+88\%$)	$r_{KD\|P}=-0.558$ (-99.92%)
	$r_{Kz\|PD}=0.299$ ($+94\%$)	$r_{KP\|Dz}=0.298$ ($+93\%$)	$r_{KD\|zP}=-0.496$ (-99.62%)
Including the full low-z subsample ($n=42$)	$r_{Kz}=0.760$ ($>99.99\%$)	$r_{KP}=0.765$ ($>99.99\%$)	$r_{KD}=-0.518$ (-99.98%)
	$r_{Kz\|P}=0.399$ ($+99.54\%$)	$r_{KP\|D}=0.743$ ($>99.99\%$)	$r_{KD\|z}=-0.455$ (-99.88%)
	$r_{Kz\|D}=0.758$ ($>99.99\%$)	$r_{KP\|z}=0.168$ ($+99\%$)	$r_{KD\|P}=-0.526$ (-99.98%)
	$r_{Kz\|PD}=0.337$ ($+98\%$)	$r_{KP\|Dz}=0.255$ ($+94\%$)	$r_{KD\|zP}=-0.487$ (-99.94%)

Table 4. Principal component analysis of emission-line gas FWHM and other radio source parameters. This analysis has been carried out on the two $z\sim1$ subsamples and either the radio power matched or full low-redshift subsamples. Other details as for Table 2.

Variable	Eigenvectors for the three matched samples				Eigenvectors including the full low-redshift data			
	1	2	3	4	1	2	3	4
FWHM	0.5554	0.1825	0.5564	0.5904	0.5553	0.1273	0.8200	0.0544
z	0.5433	−0.2665	−0.7470	−0.2753	0.5634	−0.2382	−0.2959	−0.7337
P	0.4914	−0.5362	0.3261	0.6039	0.5442	−0.3447	−0.3598	0.6750
D	−0.3936	−0.7799	−0.1613	−0.4593	−0.2794	−0.8990	0.3325	−0.0567
Percentage	61.73	22.39	8.27	7.61	67.87	23.62	5.47	3.04

the kinematics of our $z\sim1$ samples with those of galaxies with $z<0.7$ selected from the sample of Baum & McCarthy (2000). The data are strongly correlated with both redshift and radio luminosity, as well as being strongly anticorrelated with radio size. Even considered individually, the three subsamples display similar trends, although the kinematics of the low-redshift galaxies are clearly less extreme than those of their high-redshift counterparts. In the low-redshift objects, the lack of any anticorrelation between radio size and [O II] luminosity, scaled by the radio power of the host galaxy, suggests a much weaker (or perhaps non-existent) relation between emission-line strength and radio source age. It also implies that shock-induced boosting of emission-line luminosities is much less important in the low-redshift sources than for similar radio power sources (i.e. 6C galaxies) at $z\sim1$.

The variations with radio size are apparent across the full range of redshifts, and have been well documented in previous studies (e.g. Best et al. 2000b; Paper I). In general, ionization state, EELR size, velocity profile and FWHM all vary with radio size. The kinematic and ionization properties of the EELRs are found to be intrinsically correlated, despite the selection biases. It is clear that photoionization by the AGN is the only important mechanism for the more evolved, larger radio sources, which also display relatively undisturbed kinematics. The influence of shocks on the kinematics of the EELR gas clouds is certainly of importance, providing an explanation of the very distorted kinematics seen in the smaller radio sources. The clear importance of radio source shocks in these sources suggests that a gravitational origin for the observed extreme kinematics is unlikely. However, in the case of large, photoionized sources, where radio source shocks are less effective, the increased

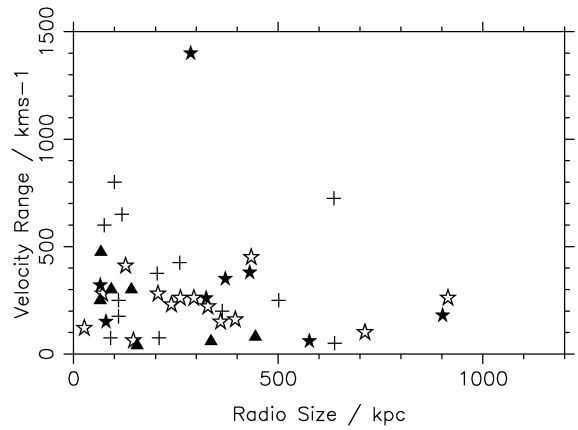

Figure 5. Variation in velocity range with radio size for three samples. Symbols as in Fig. 4.

FWHM observed at high redshifts could in fact be due to larger gravitational potentials – for example, if the radio galaxies are associated with clusters (e.g. Best 2000) rather than just the potential of an individual galaxy.

We will now consider the dependence of the ionization and kinematic properties of the EELRs on redshift and radio power independently. The inclusion of 6C data in the combined sample weakens the inherent P–z correlation rather than removing it entirely. However, using the combined sample to investigate the relationships between the EELR properties and these parameters does allow the

redshift–radio power degeneracy to be successfully broken. With this achieved, we can create a fuller picture of the processes occurring within the emission-line regions of all three subsamples of radio galaxies. The ionization state of the gas shows no significant variation with redshift, and depends only on radio power, in addition to the size of the radio source. The interplay between the strength of any shocks involved and the ionizing UV flux of the AGN is still unclear; nevertheless, the emission-line regions of the powerful $z \sim 1$ 3CR radio sources generally exist in a higher ionization state than the sources in the low-redshift or 6C subsamples, as shown by the variation of the observed [O II]/Hβ, C III] 1909-Å/C II] 2326-Å and [Ne III] 3869-Å/[Ne V] 3426-Å line ratios. The ionization state is clearly dependent on AGN properties rather than other host-galaxy properties or the environment of the radio source.

The ionization parameter U, which is proportional to the ratio of ionizing photons impinging on the surface of a cloud to the gas density, is approximately twice as great for the large 3CR radio sources as for the large 6C sources, although the distributions of sources from both subsamples cover a range of values for U (Paper I). Although the difference in ionization parameter is less than the difference in radio power between the two samples (a factor of $\sim$5 at $z \sim 1$), this anomaly could perhaps be explained by less dense clouds populating the EELRs of 6C galaxies compared with their more powerful 3CR counterparts. The sensitivity of the observations could also be an important factor. For the more powerful 3CR sources at $z \sim 1$, photoionized gas would be observable out to a greater distance from the central AGN than for the less powerful 6C sources at the same redshift. As the flux of ionizing photons impinging on a cloud per unit surface area decreases with distance from the AGN, the ionization parameter for more distant clouds will be lower than that for clouds closer to the AGN. The increase in the observed extent of the EELRs of more powerful radio sources will therefore lead to the average value of the ionization parameter being lower than that for a less powerful radio source observed to the same sensitivity. However, if the clouds are in pressure equilibrium, their density is also likely to decrease with distance from the AGN, reducing the variation in U with distance. Alternatively, the ionizing photon flux may scale non-linearly with radio luminosity, as suggested by the work of Serjeant et al. (1998) and Willott et al. (1998). They find that the optical luminosity of quasars scales roughly as $L_{\rm rad}^{0.5}$. This result suggests that the difference in ionization parameter for the two $z \sim 1$ subsamples can be expected to be less than the factor of 5 difference in their radio powers.

We also observe the effects of radio power on the kinematics of the emission-line regions, which are independently correlated with radio power once the correlations with other parameters (redshift and radio size) are removed. If the disturbed kinematics of smaller radio sources are due in the main to the influence of shocks, parameters such as the gas velocity FWHM are expected to be lower for the weaker shocks associated with less powerful radio galaxies. In addition, the more powerful radio sources may involve an increased number of jet–cloud interactions.

Finally, the observed decrease in gas velocity FWHM with redshift needs to be explained. For the kinematics, redshift is a much more important parameter than radio power, as shown by the results of the partial rank correlations and principal component analysis. This result seems to point to variations in either the host-galaxy properties, e.g. mass of gas available in the emission-line regions, or changes in, say, the IGM density with redshift. Changes in cloud sizes and/or densities would clearly affect any acceleration of the clouds due to shocks associated with the expanding radio source. An increase in jet–cloud interactions may be due to a higher gas density in the ICM for the higher-redshift galaxies. High-redshift 3CR galaxies are generally found in clusters, whereas low-redshift 3CR sources are more likely to be located in smaller groups (e.g. Hill & Lilly 1991; Best 2000). A change in radio source environment with cosmic epoch may have an effect on the observed kinematics. The more extreme kinematics of the EELRs of higher-redshift radio galaxies can plausibly be attributed in part to their richer environments as compared with low-redshift radio galaxies.

5 CONCLUSIONS

Our conclusions are as follows:

(i) A comparison between the emission-line diagnostic plots in Paper I and the current paper suggests that the shock model with a precursor model best explains the spectra of small double radio sources. The emission-line regions of larger radio sources are well explained by photoionization by the UV flux from the AGN. An accurate description of the spectra of small radio sources is likely to require a combination of both shock ionization and photoionization, even where shock ionization is likely to be the most important ionization mechanism.

(ii) In addition to the known variation in EELR gas kinematics with radio size, the kinematic properties are strongly correlated with redshift and radio power independently. The more extreme gas kinematics observed at earlier cosmic epochs suggest that the structure and/or composition of the EELR gas clouds may vary with redshift. Evolution in the environment of the radio source (e.g. changes in intergalactic medium/intracluster medium density profile) may also be occurring. The dependence of the EELR kinematics on radio power is likely to be due to the influence of shocks.

(iii) The ionization state of the gas is strongly independently correlated with radio size, as well as less strongly correlated with radio power. The data show no dependence on the redshift of the source once radio power effects have been removed. The ionization state, and hence the dominant source of ionizing photons, is therefore only dependent on the properties of the AGN (i.e. radio size and radio power) and not on cosmic epoch.

(iv) Whilst there is a fairly tight distribution of scaled $L_{[\rm O\,II]}$ with radio size in the low-redshift subsample, the weak positive correlation of these data suggests that, unlike the strong anticorrelation of emission-line luminosity with source age observed in the redshift $z \sim 1$ sources, this correlation is much weaker or non-existent for the lower-redshift radio galaxies. This indicates that shocks are less important for the radio galaxies at low redshifts, and is consistent with our other results.

ACKNOWLEDGMENTS

This work was supported in part by the Formation and Evolution of Galaxies network set up by the European Commission under contract ERB FMRX-CT96-086 of its TMR programme. We would like to thank Mark Allen for providing digitized MAPPINGSII line ratios. KJI acknowledges the support of a PPARC research studentship. PNB is grateful for the generous support offered by a Royal Society Research Fellowship. The William Herschel Telescope is operated on the island of La Palma by the Isaac Newton Group in the Spanish Observatorio del Roque de los Muchachos of the Instituto de Astrofísica de Canarias. We would like to thank the referee for useful comments.

REFERENCES

Allen M. G., Dopita M. A., Tsvetanov Z. I., 1998, ApJ, 493, 571
Baum S. A., McCarthy P. J., 2000, ApJ, 119, 2634
Baum S. A., Heckman T. M., Bridle A., van Breugel W. J. M., Miley G., 1988, ApJS, 68, 643
Baum S. A., Heckman T. M., van Breugel W. J. M., 1990, ApJS, 74, 389
Baum S. A., Heckman T. M., van Breugel W. J. M., 1992, ApJ, 389, 208
Best P. N., 2000, MNRAS, 317, 720
Best P. N., Longair M. S., Röttgering H. J. A., 1996, MNRAS, 280, L9
Best P. N., Longair M. S., Röttgering H. J. A., 1997, MNRAS, 292, 758
Best P. N., Röttgering H. J. A., Longair M. S., 1998, MNRAS, 295, 549
Best P. N., Eales S. A., Longair M. S., Rawlings S., Röttgering H. J. A., 1999, MNRAS, 303, 616
Best P. N., Röttgering H. J. A., Longair M. S., 2000a, MNRAS, 311, 1
Best P. N., Röttgering H. J. A., Longair M. S., 2000b, MNRAS, 311, 23
Best P. N., Inskip K. J., Röttgering H. J. A., Longair M. S., 2001, in Henney W. et al., eds, Emission Lines from Jet Flows, Conf. Ser. Rev. Mex. Astron. Astrofis. 13, 155
Binette L., Wilson A. S., Storchi-Bergmann T., 1996, A&A, 312, 365
Blundell K. M., Rawlings S., Willott C. J., 1999, ApJ, 117, 677
Dopita M. A., Sutherland R. S., 1996, ApJS, 102, 161
Eales S. A., 1985, MNRAS, 217, 149
Efstathiou G., Fall S. M., 1984, MNRAS, 206, 453
Hill G. J., Lilly S. J., 1991, ApJ, 367, 1
Inskip K. J., Best P. N., Rawlings S., Longair M. S., Cotter G., Röttgering H. J. A., Eales S. A., 2002, MNRAS, 337, 1381 (Paper I, this issue)
Kaiser C. R., Dennett-Thorpe J., Alexander P., 1997, MNRAS, 292, 723
Kendall M. G., 1980, Multivariate Analysis. Griffin & Co., London
Longair M. S., Best P. N., Röttgering H. J. A., 1995, MNRAS, 275, L47
McCarthy P. J., Spinrad H., van Breugel W., 1995, ApJSS, 99, 27
McCarthy P. J., Baum S. A., Spinrad H., 1996, ApJSS, 106, 281
Macklin J. T., 1982, MNRAS, 199, 1119
Neeser M. J., Eales S. A., Law-Green J. D., Leahy J. P., Rawlings S., 1995, ApJ, 451, 76
Osterbrock D. E., 1989, Astrophysics of Gaseous Nebulae and Active Galactic Nuclei. University Science Books, Mill Valley, CA
Rawlings S., Saunders R., 1991, Nat, 349, 138
Serjeant S., Rawlings S., Maddox S. J., Baker J. C., Clements D., Lacy M., Lilje P. B., 1998, MNRAS, 294, 494
Sutherland R. S., Bicknell G. V., Dopita M. A., 1993, ApJ, 414, 510
Tadhunter C. N., Morganti R. M., di Serego Alighieri S., Fosbury R. A. E., Danziger I. J., 1993, MNRAS, 263, 999
Tadhunter C. N., Morganti R., Robinson A., Dickson R., Villar-Martín M., Fosbury R. A. E., 1998, MNRAS, 298, 1035
Wall J., Peacock J., 1985, MNRAS, 216, 173
Willott C. J., Rawlings S., Blundell K. M., Lacy M., 1998, MNRAS, 300, 625

This paper has been typeset from a TEX/LATEX file prepared by the author.